

LES-STUDY OF MELT FLOW DRIVEN BY COMBINED INDUCTIVE AND CONDUCTIVE POWER SUPPLY IN METALLURGICAL MHD DEVICES

PAVLOVS¹ S., JAKOVICS¹ A., BAAKE² E., NACKE² B.

¹ Laboratory for Mathematical Modelling of Environmental and Technological Processes, University of Latvia, Zellu str. 8, LV-1002 Riga

² Institute of Electrotechnology, Leibniz University of Hannover, Wilhelm-Busch-Str. 4, D-30167 Hannover, Germany

E-mail: sergejs.pavlovs@lu.lv

Abstract: The computations of electromagnetic (EM) and hydrodynamic (HD) fields based on developed 3D model are performed for: i) almost axis-symmetrical MHD-device with bottom and submerged top electrodes with single phase alternating current (AC) and cylindrical coil around the melt; ii) MHD-device with three-phases current supplied over three submerged top electrodes as well as with EM stirrer in form of side non-symmetrical inductor, which produces “travelling” magnetic field. Obtained flow patterns are the results of competition of electro-vortex convection (EVC) and electromagnetic convection (EMC), which appear due to conductive and inductive current supply accordingly. For axis-symmetrical MHD-device the melt rotation appears as the effect of intercoupling of inductive or conductive current with magnetic fields, produced by other type of power supply.

1. Introduction

One of the popular types of industrial metallurgical equipment for melting and holding of ferrous and non-ferrous alloys (steel, ferrochrome, nichrome, etc.) uses power supply by conductive current – alternating or direct – over graphite electrodes (unsubmerged or submerged into the melt and/or slag), which have electrical contact with the melt and/or slag by arc. The heating of melt top surface may also be performed with plasma burner, thus conductive current due to jet of ionized gas is closed through the melt. The examples of such devices are electrical arc furnaces (EAF), ladle furnaces (LF), ore-melting furnaces, plasma furnaces, etc. With the purpose to intensify the circulation of melt the electromagnetic stirring (EMS) is used (for example, in LF, where EMS is the alternative to stirring with argon jet). EMS may be produced with side inductor (in LF) [1] or with bottom inductor (in EAF) [2].

Up to now the 3D numerical modelling of such MHD devices is performed for several particular cases: interaction of EMC and thermogravitational convection (TGC) [2], EM field and energy aspects [3], EVC and mixture concentration field obtained with LES (Large Eddy Simulation) approach [4], heat transfer and gas flow over slag [5]. Brief overview of recent 2D and 3D modelling may be found in [6].

The authors resume their research, performed for originally developed 2D models with application of own code [7]: the aim is 3D modelling of melt flow in MHD devices with combined inductive and conductive power supply, taking into account the intercoupling effect of interaction of electrical current with magnetic field, produced by another type of power supply. In order to eliminate TGC influence on flow structure – the result of competition of EVC, EMC and MHD-rotation – melt is considered as isothermal conductive fluid.

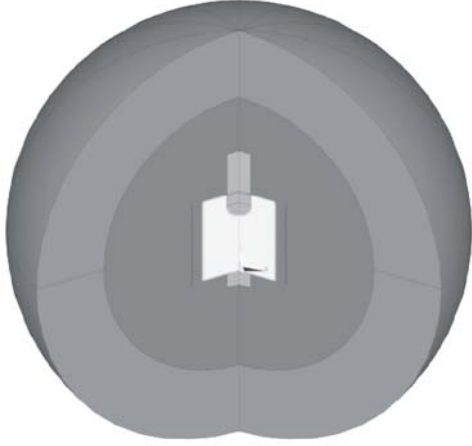


Figure 1: 3D geometry and zones of structured mesh for axis-symmetrical MHD device with submerged top and bottom AC electrodes and cylindrical single phase inductor.

Resultant *Lorentz* force in the melt [8] takes into account:

i) interaction of inductive or conductive currents with their generic magnetic fields;

ii) intercoupling of current and magnetic field produced by deferent types of power supply;

iii) phase displacement $\beta = \alpha^{el} - \alpha^{ind}$ between inductive and conductive current.

Intercoupling effects may be found in the case of equal frequency of inductive and conductive current – $\omega_{ind} = \omega_{el}$. For different frequencies $\omega_{ind} \neq \omega_{el}$ and for direct current (DC) in electrodes, time-averaged *Lorentz* force is equal zero.

1. Parameters of developed models and peculiarities of numerical computations

The geometries of developed 3D models of MHD devices with combined power supply are shown in Figures 1, 6. The geometrical, physical and operation parameters are estimated using published for advertising purposes fragmentary data [1] for industry-size LF (capacity approximately 70 t): radius and height of the melt – $r_{melt} = 1.35$ m and $h_{melt} = 3$ m; height of inductor – $h_{ind} = 3$ m; height of submerged part of electrodes – $h_{el}^{submerge} = 0.85$ m. For melt nichrome (conductivity $\sigma_{melt} = 6.7 \cdot 10^5$ S/m) and equal values of current frequency in inductor and electrodes ($f_{ind} = f_{el} = 50$ Hz) non-dimensional frequency of melt is $\hat{\omega}_{melt}^{ind} = \hat{\omega}_{melt}^{el} = 8 \cdot 10^2$.

EM field is computed with *ANSYS 14.0* in the melt, inductor and electrodes with geometries shown in Figures 1, 6. The melt turbulent flow is obtained using *ANSYS CFX 14.0* with 3D transient LES approach. As the initial distributions the results obtained with steady-state and transient Shear Stress Transport (SST) $k-\omega$ model of turbulence are used.

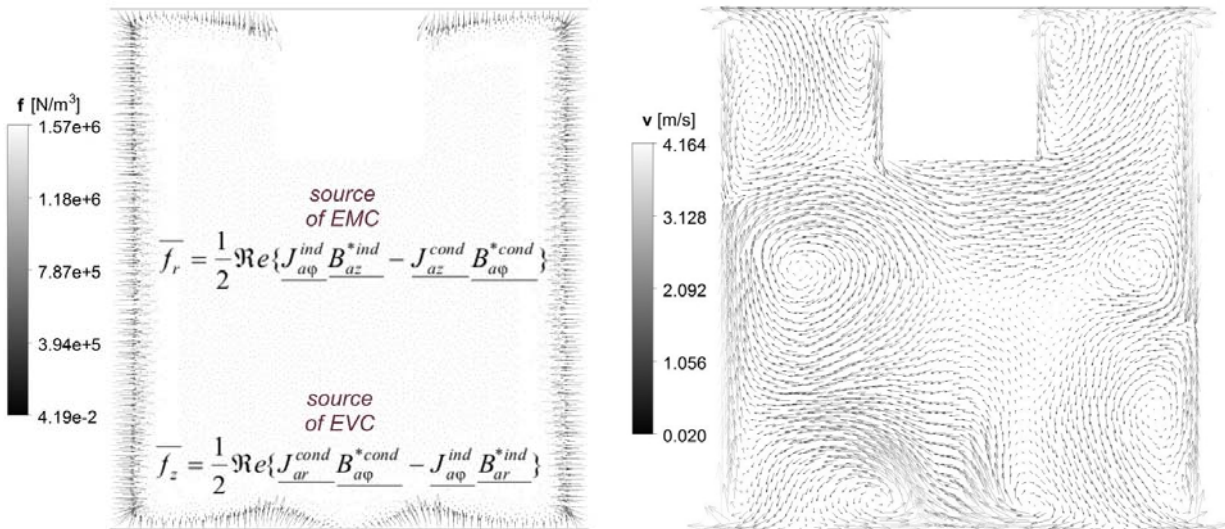


Figure 2: EM force vectors (left) and time-averaged velocity vectors (right) in vertical cross-section $y = 0$ (model in Figure 1).

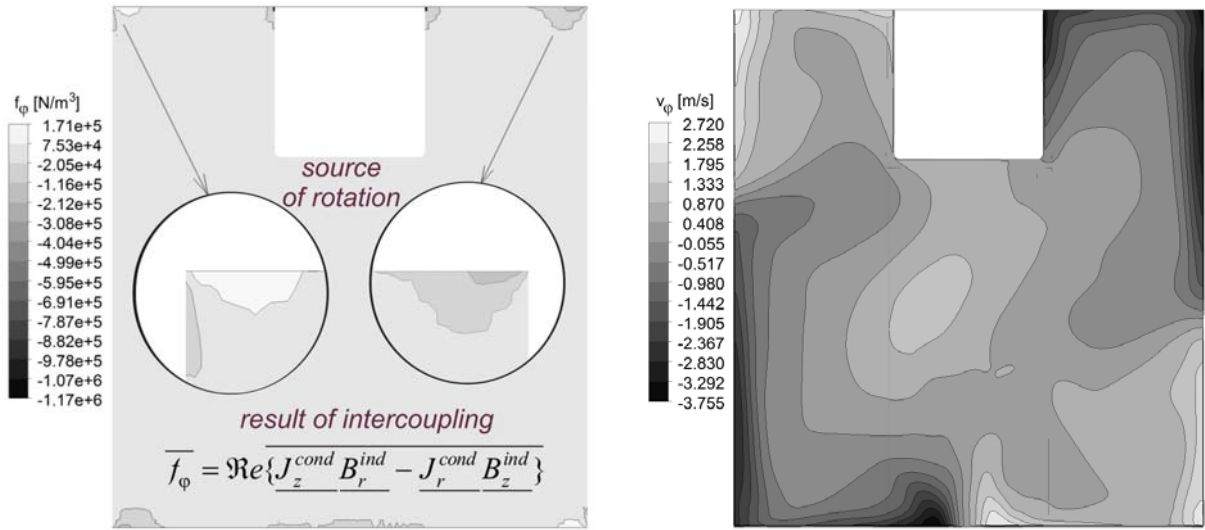


Figure 3: Isolines of azimuthal components of EM force (left) and time-averaged velocity (right) in vertical cross-section $y = 0$ (model in Figure 1).

Structured mesh (Figures 6) is built with hexahedral elements. For EM field skin layers and for HD boundary layers at solid walls the mesh with inflation is generated.

During EM modelling ~ 2.5 millions of equations for complex variables are solved. Dimension of HD mesh is ~ 2.8 millions of elements. The time step is 0.005 sec.

2. 3D model of system with top and bottom electrodes and cylindrical inductor

The main features of 3D model are the following (Figure 1):

i) *Top electrode* has submerged part; *bottom electrode* contacts the bottom of the melt. The electrodes' axes coincide with symmetrical axis of melt vessel. Phases of current in top and bottom electrodes are equal $\alpha_{top}^{el} = \alpha_{bottom}^{el} = \alpha^{el}$.

ii) *Cylindrical inductor* has azimuthal dimension $\varphi_{cylindr}^{ind} = 359^\circ$; to ensure the applying voltage drop in boundary conditions the every inductor turn has thin (1°) vertical gap. The phases of current in inductor turns are equal $\alpha_1^{ind} = \alpha_2^{ind} = \dots = \alpha_{12}^{ind} = \alpha^{ind}$.

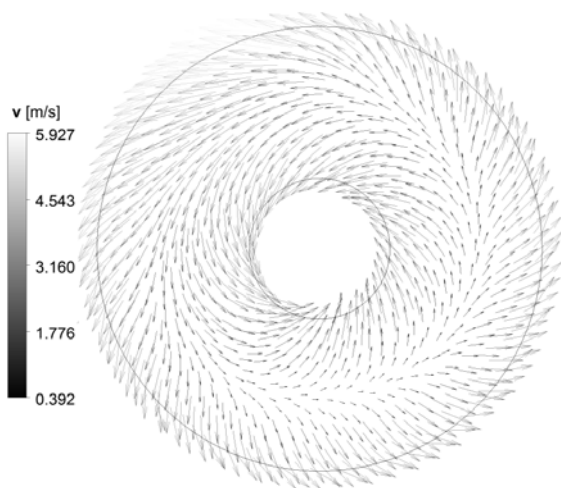


Figure 4: Time-averaged velocity vectors at melt top surface $z = 3$ m (model in Figure 1)

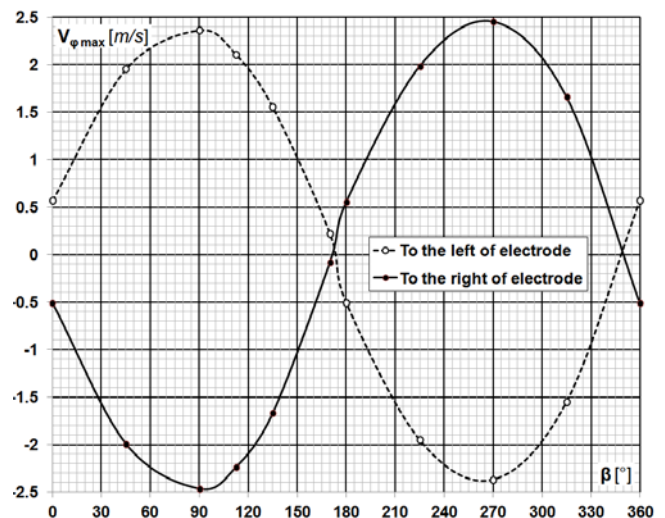


Figure 5: Maximum of azimuthal component of velocity $v_{\phi \max}$ at melt top (model in Figure 1) as the function of phase displacement β between currents in inductor and electrodes.

Characteristic distribution of resultant EM force in vertical cross-section $y=0$ is shown in Figure 2 (left). Because of noticeable skin-effect the EM force is concentrated in thin layer, which thickness is estimated with EM field penetration depth into the melt $\delta_{melt}^{ind} = \delta_{melt}^{el} \ll r_{melt}$.

EM force along cylindrical surface of melt has almost only radial component (except corner regions). The prevailing contribution to radial component \bar{f}_r , which is the main driver of EMC, gives the 1st term in upper expression, shown in Figure 2 (left). Flow patterns for system with “pure” inductor (t.i. without current over the electrodes) are typical for induction furnaces. There is not melt rotation around z-axis.

EM force along top and bottom horizontal surfaces of melt has almost only axial component (except corner regions). The prevailing contribution to axial component \bar{f}_z , which is the main driver of EVC, gives the 1st term in lower expression, shown in Figure 2 (left). Flow circulation for system with “pure” electrodes (t.i. without current in inductor) has opposite directions in comparison to EMC. There is not rotation of the melt around z-axis.

The circulation of the melt for system with combined power supply (Figure 2 (right)), is the result of competition of EMC, EVC and melt MHD-rotation around z-axis (Figure 4); phase displacement between inductive and conductive current is $\beta = 112.5^\circ$.

The melt rotation velocity $v_\varphi \sim 2.7\text{--}3.8$ m/s (Figure 3 (right)) is comparable with melt circulation velocity in meridional cross-section $v_{y=0} \sim 4.2$ m/s (Figure 2 (right)), which, in its turn, is less than total velocity at melt top $v_{top} \sim 5.9$ m/s (Figure 4). The high velocity values correspond to extreme current values in inductor and electrodes: $I_{ind} = 100$ kA; $I_{el} = 1000$ kA.

The directions of rotation in top and bottom zones of the melt are opposite (Figure 3 (right)), which coincide with directions of azimuthal component of EM force (Figure 3 (left)). The variation of phase displacement β in range from 0° to 180° makes it possible to control direction and velocity of melt rotation (Figure 5).

3. 3D model of system with three electrodes and side inductor

The main features of 3D model of system are the following (Fig. 2):

i) *Three electrodes* have submerged part with height $h_{el}^{submerge}$. Radial positions of electrodes' axes are $r_1^{el} = r_3^{el} = r_3^{el} = 0.675$ m; azimuthal positions $-\varphi_1^{el} = 0^\circ; \varphi_2^{el} = 120^\circ; \varphi_3^{el} = 240^\circ$. Phases of current in electrode are $\alpha_1^{el} = 0^\circ, \alpha_2^{el} = 120^\circ, \alpha_3^{el} = 240^\circ$.

ii) *Side inductor* with height h_{ind} has azimuthal dimension $\varphi_{side}^{ind} = 60^\circ$. Inductor produces “travelling” magnetic field. The phases of current in inductor turns are: $\alpha_1^{ind} = \dots = \alpha_4^{ind} = 0^\circ; \alpha_5^{ind} = \dots = \alpha_8^{ind} = 120^\circ; \alpha_9^{ind} = \dots = \alpha_{12}^{ind} = 240^\circ$ (numbering from bottom to top).

The 3D vectors of melt time-averaged velocity are presented in Figure 7. Inductor is turned to observer; vertical symmetry plane of model (Figure 6) is perpendicular to the page.

The EM force, which appears due to conductive current supply, is noticeable in zone around the electrodes near top of the melt. The EM force, which appears due to inductive current supply, is noticeable along cylindrical surface of the melt strait opposite to inductor, magnetic field of inductor “travels” up.

In the case of combine power supply the flow patterns, shown in Figure 7, are the result of competition of EMC and EVF and appears due to superposition of EM forces, produced by both conductive and induced current supply. Asymmetry (with respect to above mentioned vertical plane of model geometrical symmetry) of two-vortex flow in horizontal cross-section is most noticeable near top surface of the melt, where symmetrical flow of EMC competes with rotational symmetrical electro-vortex flow. Maximum value of velocity is ~ 1.2 m/s.

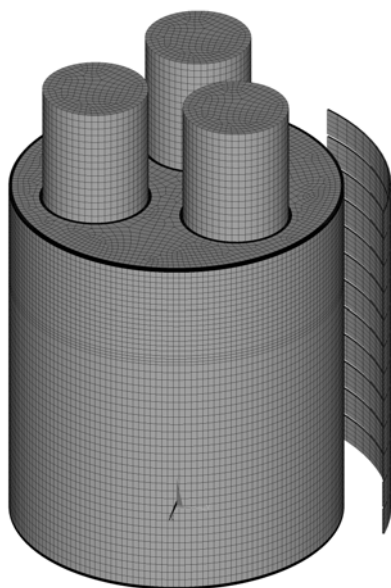


Figure 6: 3D geometry and structured mesh for MHD device with submerged three phase AC electrodes and side inductor, the source of “travelling” magnetic field.

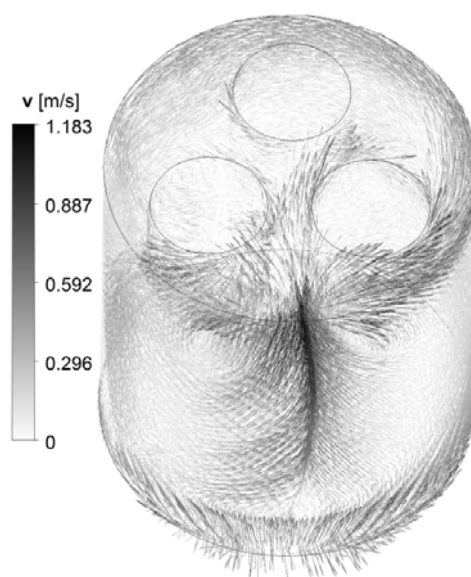


Figure 7: Time-averaged velocity 3D-vectors with “travelling” up magnetic field of inductor and phases $\alpha_1^{el} = 0^\circ$; $\alpha_2^{el} = 120^\circ$; $\alpha_3^{el} = 240^\circ$ (counter-clockwise) of current in electrodes (model in Figure 6).

4. Conclusions

The developed 3D models are universal enough for analysis of industry-size metallurgical MHD devices with conductive and inductive combined power supply in wide range of geometrical, physical and operational parameters.

The intercoupling effect (interaction of conductive current with induced magnetic field as well as interaction of induced current with magnetic field of conductive current) is illustrated with melt rotation around symmetry axis in MHD device with top and bottom single phase electrodes and cylindrical inductor.

The variation of phase displacement between inductive and conductive current makes it possible to control direction and velocity of melt rotation.

5. References

- [1] Electromagnetic stirring for ladle furnaces. Västerås (Sweden): ABB (2008).
- [2] Widlund, O.; Sand, U.; Hjortstam, O.; Zhang, X.: Modelling of electric arc furnaces (EAF) with electromagnetic stirring. Västerås (Sweden): ABB (2012).
- [3] McDougall, I.: Finite element modelling of electric currents in AC submerged arc furnaces. Proceedings of conference INFACON XI on Innovations in Ferra Alloy Industry (2007), 1–8.
- [4] Smirnov, S.A.; Kalaev, V.V.; Hekhamin, S.M.; Krutyanskii, M.M.; Kolgatin, S.N.; Nekhamin, I.S.: Mathematical simulation of electromagnetic stirring of liquid steel in a DC arc furnace. High Temperature, 48 (2010), 68–76.
- [5] Yang, Y.; Xiao, Y.; Reuter, M.A.: Analysis of transport phenomena in submerged arc furnace for ferrochrome production. Proceedings of the 10th International Ferroalloys Congress (2004), 15–25.
- [6] Jakovics, A.; Pavlovs, S.: Numerical modelling of EAF: electro-magnetic, hydrodynamic, thermal fields. In: Theory and practice of application of arc furnaces. Intensive Course Speccourse II. Edited by Nacke, B. St.Petersburg: Publishing House of ETU (2013).
- [7] Pavlov, S.I.: Numerical modelling of closed flows of conductive fluid in electromagnetic field. Summary of Ph.D. Thesis. Leningrad: Polytechnic Institute (1984) (in Russ.).
- [8] Pavlovs, S.; Jakovics, A.; Baake, E.; Nacke, B.: Melt flow patterns in metallurgical MHD devices with combined inductive and conductive power supply. Magnetohydrodynamic, (50) 2014 (in press).